

Similar curvature-to-width ratios for channels and channel belts: Implications for paleo-hydraulics of fluvial ridges on Mars

Alistair T. Hayden^{1*}, Michael P. Lamb¹ and Alexander J. Carney²

¹Division of Geological and Planetary Sciences, California Institute of Technology, 1200 E. California Boulevard, Pasadena, California 91125, USA

²Department of Mathematics, University of Rochester, RC Box 270138, Rochester, New York 14627, USA

ABSTRACT

The surface of Mars contains abundant sinuous ridges that appear similar to river channels in planform, but they stand as topographic highs. Ridges have similar curvature-to-width ratios as terrestrial meandering rivers, which has been used to support the hypothesis that ridges are inverted channels that directly reflect channel geometry. Anomalous wide ridges, in turn, have been interpreted as evidence for larger rivers on Mars compared to Earth. However, an alternate hypothesis is that ridges are exhumed channel-belt deposits—a larger zone of relatively coarse-grained deposits formed from channel lateral migration and aggradation. Here, we measured landform wavelength, radius of curvature, and width to compare terrestrial channels, terrestrial channel belts, and martian ridges. We found that all three landforms follow similar scaling relations, in which ratios of radius of curvature to width range from 1.7 to 7.3, and wavelength-to-width ratios range from 5.8 to 13. We interpret this similarity to be a geometric consequence of a sinuous curved line of finite width. Combined with observations of ridge-stacking patterns, our results suggest that wide ridges on Mars could indicate fluvial channel belts that formed over significant time rather than anomalously large rivers.

INTRODUCTION

The hydrology of ancient Mars remains poorly constrained, with major open questions about the discharge and duration of ancient river flows (e.g., Wordsworth et al., 2018; Kite, 2019). One important landform class used to reconstruct the hydraulics of rivers is fluvial ridges (Burr et al., 2010; Williams et al., 2013) (Fig. 1). Fluvial ridges are topographic highs that commonly have a sinuous or branching planform pattern that appears similar to river channels or deltas. Consequently, fluvial ridges are often called “inverted channels” (Fig. 1A), a term used to describe the topographic inversion of a channel-filling deposit that was more resistant to erosion than the surrounding material and was exhumed to produce a ridge that reflects the geometry of the original channel (e.g., Pain et al., 2007; Burr et al., 2009, 2010). The inverted-channel hypothesis has been used

to infer the discharge of ancient rivers on Mars (e.g., Burr et al., 2010; Williams et al., 2013) and interpret flow direction from the branching pattern of ridges (Lefort et al., 2012). By comparing martian fluvial ridges to terrestrial river channels of the same catchment area, Kite et al. (2019) found that martian ridges are wider and interpreted that rivers on ancient Mars must also have been larger than those on Earth today.

The inverted-channel hypothesis, however, is not the only possible interpretation of fluvial ridges. Alternatively, fluvial ridges could be eroded remnants of channel-belt deposits (Williams et al., 2009; Burr et al., 2010; DiBiase et al., 2013; Hayden et al., 2019). Channel belts are fluvial deposits built over time as rivers migrate laterally and aggrade vertically; they are commonly much wider than the channel width (e.g., Fernandes et al., 2016) and can have complex geometries of amalgamated sand and mud (e.g., Allen, 1978). Exhumation of these deposits, with preferential erosion of the mudstone

and juxtaposition of channel belts at different stratigraphic levels, has produced terrestrial ridges and ridge networks (e.g., Williams et al., 2009; Cardenas et al., 2020; Hayden and Lamb, 2020) that appear similar to examples on Mars.

Because ridge stratigraphy cannot easily be observed on Mars, it is difficult to distinguish these two formation mechanisms. Support for the inverted-channel hypothesis has come from a comparison of ridge geometry to that of terrestrial meandering rivers (e.g., Burr et al., 2010; Kite et al., 2015, 2019). In particular, meandering rivers follow scaling relations between channel-bend radius of curvature, R , or channel-bend wavelength, λ , and channel width, W :

$$\lambda = aW^b, \quad (1)$$

$$R = cW^d, \quad (2)$$

where $a = 7.5$, $b = 1.12$, $c = 1.5$, and $d = 1.12$ are empirical constants (Williams, 1988). Many ridges on Mars follow the same scaling relations, which has been used to argue that ridges are inverted channels and reflect channel dimensions (Burr et al., 2010; Kite et al., 2015, 2019). Similar arguments also have been made for interpreting ancient river deposits observed in reflectance seismology on Earth (e.g., Martin et al., 2018). We examined whether Equations 1 and 2 also describe channel belts to determine whether curvature is an unambiguous metric of ridge origin.

METHODS

We digitized landform outlines (shapefiles) from 16 river channels, 7 channel belts, and 10 sinuous ridges on Mars (Figs. 2 and 3; Table S1 in the Supplemental Material¹) to test whether

*E-mail: ahayden@caltech.edu

¹Supplemental Material. Additional description of previous work, our methods for curvature determination, a fractal geometry description of channel belts, martian ridge descriptions, and the measured data. Please visit <https://doi.org/10.1130/G48370.1> to access the supplemental material, and contact editing@geosociety.org with any questions.

CITATION: Hayden, A.T., Lamb, M.P., and Carney, A.J., 2021, Similar curvature-to-width ratios for channels and channel belts: Implications for paleo-hydraulics of fluvial ridges on Mars: *Geology*, v. 49, p. 837–841, <https://doi.org/10.1130/G48370.1>

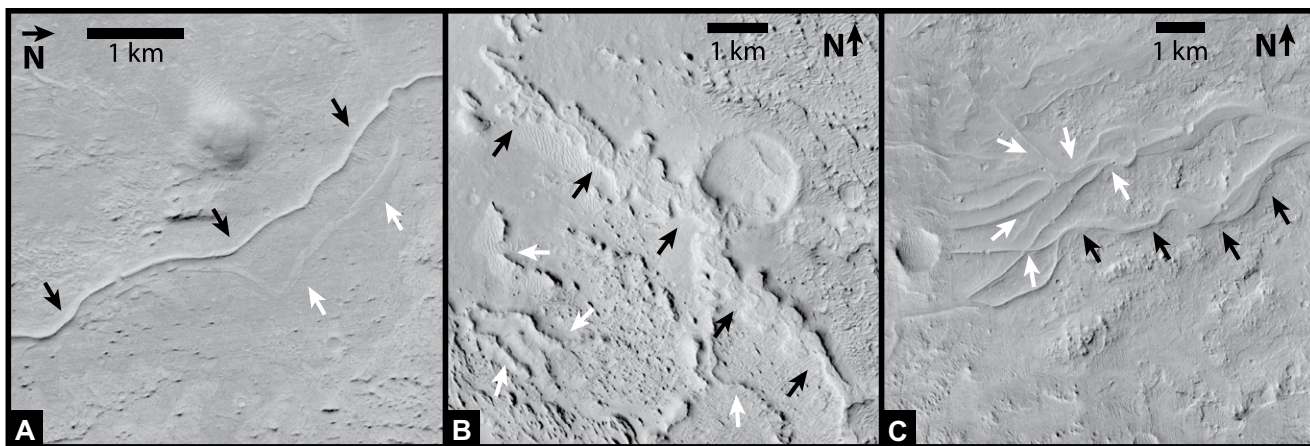


Figure 1. Sinuous ridges in Aeolis Dorsa, Mars, shown in Mars Reconnaissance Orbiter Context Camera (CTX) images (Malin et al., 2007). (A) Sinuous ridge (black arrows; Mars ridge 3 in Section S5 of the Supplemental Material [see footnote 1]) classified as “thin” and interpreted as an inverted channel (Burr et al., 2009, 2010) and stacked on a low-relief ridge (white arrows). Location: 5.63°S, 152.67°E. (B) Sinuous ridge classified as “flat” and interpreted as an exhumed channel belt (Burr et al., 2009). White arrows indicate other sinuous ridges. Location: 6.34°S, 154.15°E. (C) Sinuous ridge classified as an inverted channel (black arrows; Mars ridges 1 and 2 in Section S5 of the Supplemental Material) and used to support the observation that rivers on ancient Mars were wider than modern terrestrial rivers (Kite et al., 2019). Other ridges (white arrows) are stacked beneath the main ridge. Location: 3.03°S, 151.68°E.

channel belts follow similar scaling relations as channels. The channel-belt data set contains all published shapefiles of channel belts we could find, including of the Mississippi River (southern United States; Fernandes et al., 2016), three belts on the Rhine-Meuse Delta (Netherlands; Cohen et al., 2012), and three river corridors in Vermont (northeastern United States; Vermont Department of Environmental Conservation, 2020). Selected channels include pairs with the channel belts (Mississippi, Meuse, Nederrijn, and Waal Rivers), rivers in the Williams (1986) compilation ($n = 10$), and two additional large

North American rivers (Assiniboine and Mackenzie Rivers in Canada). Shapefiles for the Assiniboine and Mackenzie River channels were obtained from the North America Water Polygons data set (class = 1 for rivers) from Esri (<https://www.arcgis.com/home/item.html?id=1630b19fafbe4c9589306d967e418088>), and the remainder were obtained from OpenStreetMap (<https://www.openstreetmap.org/>) using its Overpass API (<https://overpass-api.de/>) downloading function. Ridges on Mars were selected from those analyzed by Kite et al. (2019) ($n = 5$) and Burr et al. (2009, 2010) ($n = 5$) in Aeolis

Dorsa (late Noachian–early Hesperian) and in Roddy, Greeley, and Chukhung craters. Selections were made based on finding well-defined caprocks in Mars Reconnaissance Orbiter Context Camera (CTX) imagery (<https://viewer.mars.asu.edu/viewer/ctx>), and the Aeolis Dorsa ridges are among the clearest examples on Mars (Burr et al., 2009). Ridge outlines were traced manually on CTX images.

We extracted centerlines and measured landform width perpendicular to the centerline from the landform shapefiles using the RivMAP package (<https://www.mathworks.com/matlabcentral/fileexchange/58264-rivmap-river-morphodynamics-from-analysis-of-planforms>; Schwenk et al., 2017). Both manual (e.g., Williams, 1986) and automated methods (e.g., Ferguson, 1975; Kite et al., 2015; Vermeulen et al., 2016) require manually digitized centerlines, which are difficult to trace precisely or consistently. To overcome these issues, we manually outlined landforms at a resolution finer than half the estimated landform width, converted it to a high-resolution binary image mask, and used RivMAP (Schwenk et al., 2017) to obtain a skeletonized centerline (Fig. 2B inset; see also the Supplemental Material). The centerline was resampled at increments equal to the median landform width, W , to avoid bias in comparisons across scales (e.g., Nikora, 1991) and to be consistent with manual measurements. To resample, we found the intersection of the skeletonized centerline and a circle of radius W drawn around the centerline start point, defined the next node in the new centerline at that intersection, and repeated the process along the landform length (Fig. 2B).

We measured radius of curvature and wavelength on the centerline for each bend. Curvature was calculated at each centerline node following Vermeulen et al. (2016) (Section S2 in the

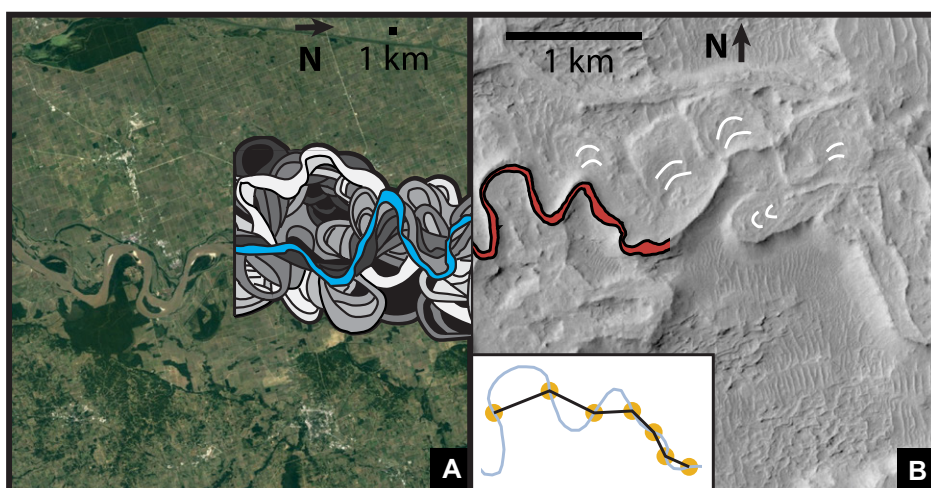


Figure 2. Examples of landforms used to measure width and curvature. (A) Image of the Mississippi River (southern United States; 36.1°N, 89.5°W; Google Earth™ image). Overlay shows active channel (blue) and channel belt, comprising many generations of amalgamated deposits (grayscale; modified after Fisk, 1945). (B) Sinuous ridge (red) stacked on a broader ridge with possible lateral accretion sets indicating channel migration (white) in Aeolis Dorsa, Mars (Mars ridge 8 in Section S5 of the Supplemental Material [see footnote 1]) (Mars Reconnaissance Orbiter Context Camera [CTX] image; 154.878°E, 4.92°S). Inset shows centerline (blue) automatically extracted from red ridge segment; yellow dots are curvature-inflection points; black line segments denote half-wavelength ($\lambda/2$).

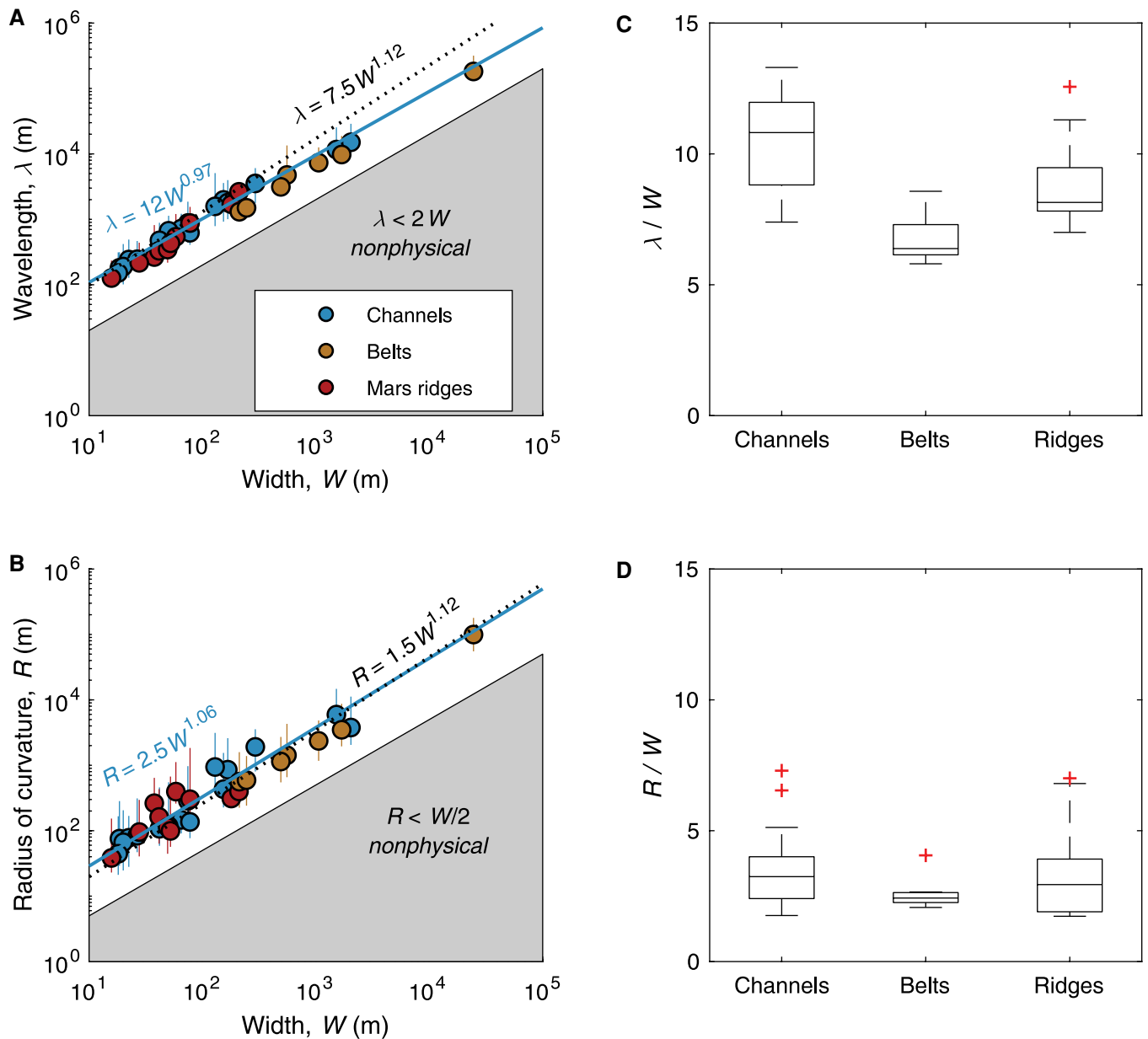


Figure 3. Comparison of landform wavelength and radius of curvature to width (Table S1 [see footnote 1]). (A,B) Each dot represents median values for one landform, with error bars (commonly smaller than marker size) representing 5th–95th percentile range. Solid blue lines are reduced-major-axis best fits to terrestrial river channel data, and dashed black lines are Williams (1986) relations. Gray area is nonphysical by Equations 3 and 4. (C,D) Box-and-whisker plots of ratio between wavelength or radius of curvature and width. Each box spans the 25th–75th percentile of the data; horizontal lines represent medians, and whiskers span the remaining data, except for outliers (indicated by red crosses).

Supplemental Material). Zero-crossings in curvature defined the boundaries between individual bends (Ferguson, 1975), and we calculated meander wavelength as twice the straight-line distance in plan view between each crossing (e.g., Kite et al., 2015; Fig. 2B). The radius of curvature was calculated as the inverse of the maximum curvature for each bend because it approximates prior methods of fitting circles to the tightest bend (e.g., Vermeulen et al., 2016). We took the median values of radius of curvature, R , and wavelength, λ , for each landform. Our method compares within a factor of three of W , R , and λ values measured manually by Williams (1986) (Fig. S2).

RESULTS

We identified and analyzed 1336 bends from river channels, 312 from channel belts, and 194 from martian fluvial ridges. Channels have median widths of 18–2000 m, channel belts have widths of 210–25,000 m, and ridges have widths of 16–210 m (Figs. 3A and 3B). The channel belts are, on average, wider than the channels, as expected, and they both follow a similar scaling relation with channel width. Wavelength and radius of curvature follow similar power-law relations (Equations 1 and 2) for all three landforms with best-fit (using reduced-major-axis fitting to the data in log space) b and d values equal to 0.97 and 1.06 for channels,

1.03 and 1.1 for channel belts, and 1.19 and 0.98 for ridges. The data follow the relation proposed by Williams (1986) except for cases with $W > 300$ m (Figs. 3A and 3B). We also calculated the ratios λ/W and R/W because b and d are near unity. The median (and interquartile range) of λ/W are 10.8 (8.8–12) for channels, 6.4 (6.1–7.3) for channel belts, and 8.2 (7.8–9.5) for martian ridges (Fig. 3C). The median (and range) of R/W are 3.2 (2.4–4.0) for channels, 2.4 (2.3–2.6) for channel belts, and 2.9 (1.9–3.9) for ridges (Fig. 3D). Although channels tend to have slightly larger median values of λ/W and R/W compared to channel belts, the distributions overlap substantially, making

these metrics undiagnostic of whether ridges are channels or channel belts.

The reason for similar scaling between river channels, channel belts, and ridges is that geometrically they all are sinuous lines with a finite width, which places lower limits on λ/W and R/W (Fig. 3). For instance, if a landform's centerline has a radius of curvature smaller than half its width, its edges would contact each other and there would no longer be a recognizable centerline, such that

$$R \geq W/2. \quad (3)$$

Similarly, for a centerline discretized with post-spacing equal to the width, the edges would contact when the straight-line distance between bend end points ($\lambda/2$ by definition) decreased to the width, such that

$$\lambda/2 \geq W. \quad (4)$$

If bends along the landforms were all identical to the lower limits given by Equations 3 and 4, then the landforms would be tight, repeating curves. In reality, the curvature of rivers and channel belts is fractal (e.g., Nikora, 1991; Montgomery, 1996; Section S4), and therefore the wavelength and curvature values occur at many scales above the cutoff scale (Vermeulen et al., 2016) (Figs. S1, S4–S11), which increases the median values away from the lower bounds. However, the fractal nature also means that each large curve comprises many smaller curves (Vermeulen et al., 2016), so the abundance of small curves weights the median values toward the lower bounds.

DISCUSSION

Our results show that channel belts and channels follow similar scaling relations with landform width, and both have similar scaling relations to martian ridges. Although Kolmogorov-Smirnov tests (Section S3) can distinguish the distributions of channels and channel belts for λ/W , they cannot for R/W , and the similarity between the distributions, nonetheless, makes them ambiguous metrics for discerning whether an individual ridge is a channel or channel belt. Slight differences in the λ/W distributions (Fig. 3C) could be due to different formation histories between channels and channel belts. Channel belts also have more spatial variability in their widths (e.g., Fig. 2A), which could lead to short-wavelength oscillations in the centerline. The R/W ratio tends more strongly toward the minimum value (Equation 3) and therefore is similar across all landforms (Fig. 3D). The overall similarity in R/W and λ/W ratios across landforms necessitates reevaluation of interpretations where the similarity was used to interpret martian ridges as direct proxies for fluvial channels.

Ridges on Mars can exceed 1 km width; those examined by Kite et al. (2019) are wider by up to a factor of twenty compared to terrestrial channels with similar catchment areas, which was interpreted to represent rivers with extraordinary widths and discharges as compared to those on Earth. A simpler explanation might be that these landforms are exhumed channel belts (e.g., Burr et al., 2010; DiBiase et al., 2013; Cardenas et al., 2018; Davis et al., 2019). Because channel belts form over time due to channel lateral migration, they can be as much as 30-fold wider than their associated channels (Hayden et al., 2019).

On Earth, lateral accretion sets deposited during channel migration are hallmarks of channel belts (Mohrig et al., 2000). Although a few examples exist from Mars orbital imagery (e.g., Burr et al., 2009; Cardenas et al., 2018; Fig. 2B; Figs. S9 and S10), there is a lack of the ground-based observations necessary to observe cross strata in ridges on Mars. However, stacked coarse-grained channel belts within a fine-grained floodplain matrix define the typical stratigraphic architecture of fluvial sedimentary deposits (e.g., Allen, 1978; Bridge and Leeder, 1979). On Mars, stacked ridges have been observed (DiBiase et al., 2013; Cardenas et al., 2018; Davis et al., 2019), commonly in association with “flat” ridges (e.g., Burr et al., 2009, 2010; Kite et al., 2015), in support of the channel-belt hypothesis. Many, but not all, of the ridges that we analyzed are stacked (Figs. 1A, 1C and 2B). In contrast, channel fills that preserve channel geometry are rare in fluvial stratigraphy; they tend to be fine grained as a result of overbank sedimentation into an abandoned channel (e.g., Nichols and Fisher, 2007) and are therefore unlikely to be more erosion resistant than the surrounding material to form ridges. Non-fluvial channel fills, such as lava flows, are also plausible (e.g., Burr et al., 2010), but these typically fill valleys or canyons (e.g., Stearns, 1936), such that they also would yield ridges wider than the channels.

If martian ridges are indeed exhumed channel belts rather than inverted channels, then ridge width and wavelength should reflect channel-belt geometry rather than channel geometry. In this case, the bankfull discharge of ancient martian rivers could be significantly smaller than that calculated with the assumption that ridge width and wavelength reflect the channel geometry, though some terrestrial exhumed channel belts have similar dimensions to paleochannels due to narrowing by erosion (Hayden et al., 2019; Hayden and Lamb, 2020). Furthermore, while ridges are interpreted to represent a preserved fluvial landscape at a snapshot in time under the inverted-channel hypothesis (DiBiase et al., 2013), channel belts are fluvial deposits accumulated over thousands of years (e.g., Törnqvist et al., 1996). Moreover, thick

sequences of fluvial deposits with stacked channel belts, similar to those on Mars (e.g., DiBiase et al., 2013; Kite et al., 2015), form on Earth over hundreds of thousands to millions of years (e.g., Johnson et al., 1985).

CONCLUSIONS

River channels, channel belts, and martian ridges are all sinuous landforms with a finite width, and they all have similar scaling relations between radius of curvature, R , and landform width, W , and between wavelength, λ , and width. Our results indicate that $R-W$ and $\lambda-W$ scaling relations should not be used to interpret whether martian ridges represent inverted channels or exhumed channel belts. Channel belts are larger than channels because they form over time due to river lateral migration, and their deposits are a fundamental element of fluvial stratigraphic architecture. Therefore, large martian ridges might represent exhumed channel belts representing river activity over substantial time, rather than extraordinarily large rivers.

ACKNOWLEDGMENTS

This work was supported by NASA (grant NNX16G to Lamb and graduate fellowship 80NSSC17K0492 to Hayden). The manuscript benefited greatly from feedback from John Swartz and two anonymous reviewers.

REFERENCES CITED

- Allen, J.R.L., 1978, Studies in fluvial sedimentation: An exploratory quantitative model for the architecture of avulsion-controlled alluvial suites: *Sedimentary Geology*, v. 21, p. 129–147, [https://doi.org/10.1016/0037-0738\(78\)90002-7](https://doi.org/10.1016/0037-0738(78)90002-7).
- Bridge, J.S., and Leeder, M.R., 1979, A simulation model of alluvial stratigraphy: *Sedimentology*, v. 26, p. 617–644, <https://doi.org/10.1111/j.1365-3091.1979.tb00935.x>.
- Burr, D.M., Enga, M.-T., Williams, R.M.E., Zimbelman, J.R., Howard, A.D., and Brennand, T.A., 2009, Pervasive aqueous paleoflow features in the Aeolis/Zephyria Plana region, Mars: *Icarus*, v. 200, p. 52–76, <https://doi.org/10.1016/j.icarus.2008.10.014>.
- Burr, D.M., Williams, R.M.E., Wendell, K.D., Chojnacki, M., and Emery, J.P., 2010, Inverted fluvial features in the Aeolis/Zephyria Plana region, Mars: Formation mechanism and initial paleodischarge estimates: *Journal of Geophysical Research*, v. 115, E07011, <https://doi.org/10.1029/2009JE003496>.
- Cardenas, B.T., Mohrig, D., and Goudge, T.A., 2018, Fluvial stratigraphy of valley fills at Aeolis Dorsa, Mars: Evidence for base-level fluctuations controlled by a downstream water body: *Geological Society of America Bulletin*, v. 130, p. 484–498, <https://doi.org/10.1130/B31567.1>.
- Cardenas, B.T., Mohrig, D., Goudge, T.A., Hughes, C.M., Levy, J.S., Swanson, T., Mason, J., and Zhao, F., 2020, The anatomy of exhumed river-channel belts: Bedform to belt-scale river kinematics of the Ruby Ranch Member, Cretaceous Cedar Mountain Formation, Utah, USA: *Sedimentology*, v. 67, p. 3655–3682, <https://doi.org/10.1111/sed.12765>.
- Cohen, K.M., Stouthamer, E., Pierik, H.J., and Geurts, A.H., 2012, Digitaal basisbestand paleogeografie van de Rijn-Maas delta: Utrecht, Universiteit

- Utrecht, Department Fysische Geografie, digital dataset, <https://doi.org/10.17026/dans-x7g-sjtw>.
- Davis, J.M., Gupta, S., Balme, M., Grindrod, P.M., Fawdon, P., Dickson, Z.I., and Williams, R.M.E., 2019, A diverse array of fluvial depositional systems in Arabia Terra: Evidence for mid-Noachian to early Hesperian rivers on Mars: *Journal of Geophysical Research: Planets*, v. 124, p. 1913–1934, <https://doi.org/10.1029/2019JE005976>.
- DiBiase, R.A., Limaye, A.B., Scheingross, J.S., Fischer, W.W., and Lamb, M.P., 2013, Delta deposits at Aeolis Dorsa: Sedimentary evidence for a standing body of water on the northern plains of Mars: *Journal of Geophysical Research: Planets*, v. 118, p. 1285–1302, <https://doi.org/10.1002/jgre.20100>.
- Ferguson, R.I., 1975, Meander irregularity and wavelength estimation: *Journal of Hydrology (Amsterdam)*, v. 26, p. 315–333, [https://doi.org/10.1016/0022-1694\(75\)90012-8](https://doi.org/10.1016/0022-1694(75)90012-8).
- Fernandes, A.M., Törnqvist, T.E., Straub, K.M., and Mohrig, D., 2016, Connecting the backwater hydraulics of coastal rivers to fluvio-deltaic sedimentology and stratigraphy: *Geology*, v. 44, p. 979–982, <https://doi.org/10.1130/G37965.1>.
- Fisk, H.N., 1945, Geological investigation of the alluvial valley of the lower Mississippi River: Vicksburg, Mississippi, U.S. Army Corps of Engineers, Mississippi River Commission, 78 p.
- Hayden, A.T., and Lamb, M.P., 2020, Fluvial sinuous ridges of the Morrison Formation, USA: Meandering, scarp retreat, and implications for Mars: *Journal of Geophysical Research: Planets*, v. 125, e2020JE006470, <https://doi.org/10.1029/2020JE006470>.
- Hayden, A.T., Lamb, M.P., Fischer, W.W., Ewing, R.C., McElroy, B.J., and Williams, R.M.E., 2019, Formation of sinuous ridges by inversion of river-channel belts in Utah, USA, with implications for Mars: *Icarus*, v. 332, p. 92–110, <https://doi.org/10.1016/j.icarus.2019.04.019>.
- Johnson, N.M., Stix, J., Tauxe, L., Cervený, P.F., and Tahirkheli, R.A., 1985, Paleomagnetic chronology, fluvial processes, and tectonic implications of the Siwalik deposits near Chinji village, Pakistan: *The Journal of Geology*, v. 93, p. 27–40, <https://doi.org/10.1086/628917>.
- Kite, E.S., 2019, Geologic constraints on early Mars climate: *Space Science Reviews*, v. 215, 10, <https://doi.org/10.1007/s11214-018-0575-5>.
- Kite, E.S., Howard, A.D., Lucas, A., and Lewis, K.W., 2015, Resolving the era of river-forming climates on Mars using stratigraphic logs of river-deposit dimensions: *Earth and Planetary Science Letters*, v. 420, p. 55–65, <https://doi.org/10.1016/j.epsl.2015.03.019>.
- Kite, E.S., Mayer, D.P., Wilson, S.A., Davis, J.M., Lucas, A.S., and de Quay, G.S., 2019, Persistence of intense, climate-driven runoff late in Mars history: *Science Advances*, v. 5, eaav7710, <https://doi.org/10.1126/sciadv.aav7710>.
- Lefort, A., Burr, D.M., Beyer, R.A., and Howard, A.D., 2012, Inverted fluvial features in the Aeolis-Zephyria Plana, western Medusae Fossae Formation, Mars: Evidence for post-formation modification: *Journal of Geophysical Research: Planets*, v. 117, E03007, <https://doi.org/10.1029/2011JE004008>.
- Malin, M.C., et al., 2007, Context Camera investigation on board the Mars Reconnaissance Orbiter: *Journal of Geophysical Research*, v. 112, E05S04, <https://doi.org/10.1029/2006JE002808>.
- Martin, J., Fernandes, A.M., Pickering, J., Howes, N., Mann, S., and McNeil, K., 2018, The stratigraphically preserved signature of persistent backwater dynamics in a large paleodelta system: The Mungaroo Formation, North West Shelf, Australia: *Journal of Sedimentary Research*, v. 88, p. 850–872, <https://doi.org/10.2110/jsr.2018.38>.
- Mohrig, D., Heller, P.L., Paola, C., and Lyons, W.J., 2000, Interpreting avulsion process from ancient alluvial sequences: Guadalupe-Matarranya system (northern Spain) and Wasatch Formation (western Colorado): *Geological Society of America Bulletin*, v. 112, p. 1787–1803, [https://doi.org/10.1130/0016-7606\(2000\)112<1787:IA PFAA>2.0.CO;2](https://doi.org/10.1130/0016-7606(2000)112<1787:IA PFAA>2.0.CO;2).
- Montgomery, K., 1996, Sinuosity and fractal dimension of meandering rivers: *Area*, v. 28, p. 491–500, <https://www.jstor.org/stable/20003734>.
- Nichols, G.J., and Fisher, J.A., 2007, Processes, facies and architecture of fluvial distributary system deposits: *Sedimentary Geology*, v. 195, p. 75–90, <https://doi.org/10.1016/j.sedgeo.2006.07.004>.
- Nikora, V.I., 1991, Fractal structures of river plan forms: *Water Resources Research*, v. 27, p. 1327–1333, <https://doi.org/10.1029/91WR00095>.
- Pain, C.F., Clarke, J.D.A., and Thomas, M., 2007, Inversion of relief on Mars: *Icarus*, v. 190, p. 478–491, <https://doi.org/10.1016/j.icarus.2007.03.017>.
- Schwenk, J., Khandelwal, A., Fratkin, M., Kumar, V., and Fofoula-Georgiou, E., 2017, High spatiotemporal resolution of river planform dynamics from Landsat: The RivMAP toolbox and results from the Ucayali River: *Earth and Space Science (Hoboken, N.J.)*, v. 4, p. 46–75, <https://doi.org/10.1002/2016EA000196>.
- Stearns, H.T., 1936, Origin of the large springs and their alcoves along the Snake River in southern Idaho: *The Journal of Geology*, v. 44, p. 429–450, <https://doi.org/10.1086/624441>.
- Törnqvist, T.E., Kidder, T.R., Autin, W.J., van der Borg, K., de Jong, A.F.M., Klerks, C.J.W., Snijders, E.M.A., Storms, J.E.A., van Dam, R.L., and Wiemann, M.C., 1996, A revised chronology for Mississippi River subdeltas: *Science*, v. 273, p. 1693–1696, <https://doi.org/10.1126/science.273.5282.1693>.
- Vermeulen, B., Hoitink, A.J.F., Zolezzi, G., Abad, J.D., and Aalto, R., 2016, Multiscale structure of meanders: *Geophysical Research Letters*, v. 43, p. 3288–3297, <https://doi.org/10.1002/2016GL068238>.
- Vermont Department of Environmental Conservation, 2020, River corridor and floodplain maps: <https://dec.vermont.gov/watershed/rivers/river-corridor-and-floodplain-protection/river-corridor-and-floodplain-maps> (accessed September 2019).
- Williams, G.P., 1986, River meanders and channel size: *Journal of Hydrology (Amsterdam)*, v. 88, p. 147–164, [https://doi.org/10.1016/0022-1694\(86\)90202-7](https://doi.org/10.1016/0022-1694(86)90202-7).
- Williams, G.P., 1988, Paleofluvial estimates from dimensions of former channels and meanders, in Baker, V.R., et al., eds., *Flood Geomorphology*: New York, John Wiley & Sons, p. 321–334.
- Williams, R.M.E., Irwin, R.P., III, and Zimbelman, J.R., 2009, Evaluation of paleohydrologic models for terrestrial inverted channels: Implications for application to martian sinuous ridges: *Geomorphology*, v. 107, p. 300–315, <https://doi.org/10.1016/j.geomorph.2008.12.015>.
- Williams, R.M.E., Irwin, R.P., III, Burr, D.M., Harrison, T., and McClelland, P., 2013, Variability in martian sinuous ridge form: Case study of Aeolis Serpens in the Aeolis Dorsa, Mars, and insight from the Mirackina paleoriver, South Australia: *Icarus*, v. 225, p. 308–324, <https://doi.org/10.1016/j.icarus.2013.03.016>.
- Wordsworth, R., Ehlmann, B., Forget, F., Haberle, R., Head, J., and Kerber, L., 2018, Healthy debate on early Mars: *Nature Geoscience*, v. 11, p. 888–888, <https://doi.org/10.1038/s41561-018-0267-5>.

Printed in USA